Ecosystems (2009) 12: 261–278
DOI: 10.1007/s10021-008-9221-5

ECOSYSTEMS


# Environmental and Biotic Controls over Aboveground Biomass Throughout a Tropical Rain Forest

Gregory P. Asner,[1]* R. Flint Hughes,[2] Timothy A. Varga,[1] David E. Knapp,[1] and Ty Kennedy-Bowdoin[1]

[1]*Department of Global Ecology, Carnegie Institution, 260 Panama Street, Stanford, California 94305, USA;* [2]*Institute of Pacific Islands Forestry, USDA Forest Service, 60 Nowelo Street, Hilo, Hawaii 96720, USA*

## Abstract

The environmental and biotic factors affecting spatial variation in canopy three-dimensional (3-D) structure and aboveground tree biomass (AGB) are poorly understood in tropical rain forests. We combined field measurements and airborne light detection and ranging (lidar) to quantify 3-D structure and AGB across a 5,016 ha rain forest reserve on the northeastern flank of Mauna Kea volcano, Hawaii Island. We compared AGB among native stands dominated by *Metrosideros polymorpha* found along a 600–1800 m elevation/climate gradient, and on three substrate-age classes of 5, 20, and 65 kyr. We also analyzed how alien tree invasion, canopy species dominance and topographic relief influence AGB levels. Canopy vertical profiles derived from lidar measurements were strong predictors ($r^2$ = 0.78) of AGB across sites and species. Mean AGB ranged from 48 to 363 Mg ha$^{-1}$ in native forest stands. Increasing elevation corresponded to a 53–84% decrease in AGB levels, depending upon substrate age. Holding climate constant, changes in substrate age from 5 to 65 kyr corresponded to a 23–53% decline in biomass. Invasion by *Psidium cattleianum* and *Ficus rubiginosa* trees resulted in a 19–38% decrease in AGB, with these carbon losses mediated by substrate age. In contrast, the spread of former plantation tree species *Fraxinus uhdei* corresponded to a 7- to 10-fold increase in biomass. The effects of topographic relief at both local and regional scales were evident in the AGB maps, with poorly drained terrain harboring 76% lower biomass than forests on well-drained relief. Our results quantify the absolute and relative importance of environmental factors controlling spatial variation in tree biomass across a rain forest landscape, and highlight the rapid changes in carbon storage incurred following biological invasion.

**Key words:** airborne remote sensing; alien invasive species; biological invasion; carbon storage; Hawaii; lidar; light detection and ranging; substrate age; tropical forest; vegetation structure.

Received 21 March 2008; accepted 18 November 2008;
published online 13 December 2008

**Electronic supplementary material:** The online version of this article (doi:10.1007/s10021-008-9221-5) contains supplementary material, which is available to authorized users.

**Author Contributions:** GPA and RFH conceived of or designed the study. GPA, RFH, TAV, DEK, and TKB performed research and analyzed data. GPA, RFH, DEK, and TKB contributed new methods or models. GPA wrote the article.

**Corresponding author; e-mail:* gpa@stanford.edu

## Introduction

Aboveground tree biomass (hereafter 'AGB') in a forest integrates processes of plant establishment, growth and mortality, as well as succession, disturbance, and ecosystem processes. Forest AGB is also influenced by climate, substrate age and soil fertility, species composition, and topographic relief

(for example, Laurance and others 1999). However, our understanding of the factors most important to predicting AGB levels remains limited because we have lacked the ability to measure biomass across landscapes while, at the same time, maintaining high spatial and biophysical resolution. To do so would allow us to assess the relative importance of environmental and biotic controls in a way that has not been possible using ground-based measurements alone. The basic ecological insight derived from landscape-scale measurements would then aid in prediction of biomass levels in the context of carbon sequestration and climate change mitigation (Clark 2002; Phillips and others 2002).

The literature provides plot-scale estimates of biomass across a range of tropical forests (for example, Phillips and others 1998) and local land-use gradients (for example, Hughes and others 2002). At the plot level, AGB estimates are usually developed from hand-measured tree diameters, sometimes with canopy height (CH) and wood density measurements to improve accuracy (Chave and others 2005). However, AGB remains poorly quantified beyond the hectare scale in most tropical forests, owing to the structural and biotic complexity of these systems (Brown and Lugo 1984; Chave and others 2005). The relevance of plot-based biomass estimates are thus limited by spatial variation in species composition, disturbance history, and environmental controls such as climate and substrate type, making it difficult to extrapolate to larger geographic scales.

In recent years, AGB mapping approaches have been advanced using airborne multispectral, lidar (light detection and ranging) and radar technologies (Lefsky and others 2002b; Treuhaft and others 2004; Brown and others 2005; Palace and others 2008). Both small ($<5$ m) and large ($>25$ m) footprint lidar have been most heavily used to estimate forest carbon (for example, Drake and others 2002; Lefsky and others 2002a; Popescu and others 2004; Lefsky and others 2005). Despite the rapidly expanding use of lidar for forest structural and biomass studies, few have applied the measurements to answer fundamental ecological questions. Instead, most studies have focused on the lidar methods and analysis steps, which are fortunately now deemed sufficient for application to a variety of ecological questions (reviewed by Lefsky and others 2002b).

In ecosystem studies conducted throughout the Hawaiian Islands, variation in environmental conditions have been successfully accounted for in plot-level studies of soil development, nutrient availability, and plant productivity (Vitousek 2004). Parent material can be held constant because Hawaiian substrates are derived from a common volcanic source. Precipitation and temperature vary predictably based on elevation and aspect, with lower-elevation windward forest sites being warm and wet compared to cooler (and often drier) sites at higher elevations (Giambelluca and others 1986). Lava flows are sufficiently dated to provide control over substrate ages ranging from days to over 4.1 M years (Stearns 1985). Relief can be locally controlled on remnant volcanic shield surfaces (Crews and others 1995; Vitousek and others 1997), and both hillslope and microsite terrain variations can be controlled for at the landscape level (Chadwick and others 1999; Porder and others 2005). Although much control can be applied to ecological studies in Hawaii, few have considered the relative importance of environmental drivers of biomass change (but see Raich and others 1997). Moreover, alien invasive plants are rapidly changing the composition of many Hawaiian forests (Smith 1985; Asner and others 2008), challenging studies of how changes in species dominance alter ecosystem structure and function. Biological invasions may increase, decrease, or sustain pre-invasion AGB, depending on the particular growth form and functional characteristic of the invader (Ehrenfeld 2003), but few studies have addressed the sign and magnitude of change in AGB following invasion (Vitousek 2004). No studies document such changes at the landscape-scale.

Despite the work done on Hawaiian ecosystem development and dynamics, we know little of how AGB varies among combinations of climate, relief, substrate age, and biological invasion. Integrated field and airborne measurements could facilitate regional carbon-storage assessments across a range of environmental conditions, but the methods have not been tested and applied in Hawaiian forests. Understanding environmental controls on aboveground biomass, and the effects of biological invasion on carbon stocks, is needed to predict changes in landscape-level carbon storage and sequestration potential.

This study combined plot measurements and airborne lidar to map canopy structure and biomass across an array of forest stands in northeastern Hawaii Island. Specifically, we sought to answer three questions focused on the environmental and biotic factors affecting AGB at the landscape level: (i) Can airborne lidar measurements of canopy 3-D structure be used to estimate AGB, independent of canopy species composition, in Hawaiian rain for-

ests? (ii) Does AGB vary more by substrate age (here, 5–65 + kyr) or by climate (range of 1500 mm $y^{-1}$ and 5°C) in Hawaiian rain forests? (iii) Do forests dominated by invasive tree species store more or less carbon than native stands in similar substrate, relief, and climate zones? The airborne lidar coverage generated for this study also provided an opportunity to consider effects of major topographic relief changes and native forest canopy dominance on aboveground carbon storage.

## Materials and Methods

### Study Area

Our study focused on the 5,016 ha State of Hawaii Hilo Forest Reserve and Laupahoehoe Natural Area Reserve on the northeast flank of Mauna Kea volcano (Figure 1). This forest is also designated as the Hawaii Experimental Tropical Forest (HETF) of the US Forest Service, and is selected for the Pacific regional domain of the National Ecological Observatory Network (http://www.neoninc.org). The study forest extends from 600 m to more than 1800 m elevation (Figure 2), with a resulting mean annual precipitation and temperature gradient of approximately 2000–3500 mm $y^{-1}$ and 13–18°C, respectively (Giambelluca and others 1986). There are also three distinct substrate-age classes found throughout the reserve: 5 ky (ky = 1,000 y) substrate covering 2471 ha; 20 ky over 797 ha; and 65 + ky encompassing 1748 ha (Figure 2). The airborne lidar coverage also included a 747 ha area of poorly drained terrain caused by a change in slope shown in geomorphological maps of Mauna Kea volcano (Armstrong 1983).

Canopy species dominance varies spatially in several well-known ways throughout this forest. At the broadest spatial extent, the canopy is dominated by keystone native Hawaiian tree species *Metrosideros polymorpha* (Myrtaceae), which can be found in large contiguous forest patches at all elevations and on most substrates (Figure 2). In addition, at elevations of 1400–1500 m, there is a 131 ha area dominated by *M. polymorpha* trees that have undergone natural dieback (Mueller-Dombois 1987), providing a comparison of biomass measures between live and dead canopies. Specific areas, mostly at higher elevations (1400, 1600 m) are dominated by the native nitrogen-fixing tree, *Acacia koa* (Leguminaceae), or the alien tree, *Fraxinus uhdei* (Oleaceae); the latter was planted as a potential timber species in the 1920s and then abandoned (Francis 1990; Rothstein and others 2004). There is also a zone of biological invasion at 700–900 m elevation caused by the fast-growing trees *Psidium cattleianum* (Myrtaceae) and *Ficus rubiginosa* (Moraceae) (Asner and others 2008). The poorly drained terrain is dominated by *M. polymorpha* but with a more open canopy (http://pbin.nbii.gov/).

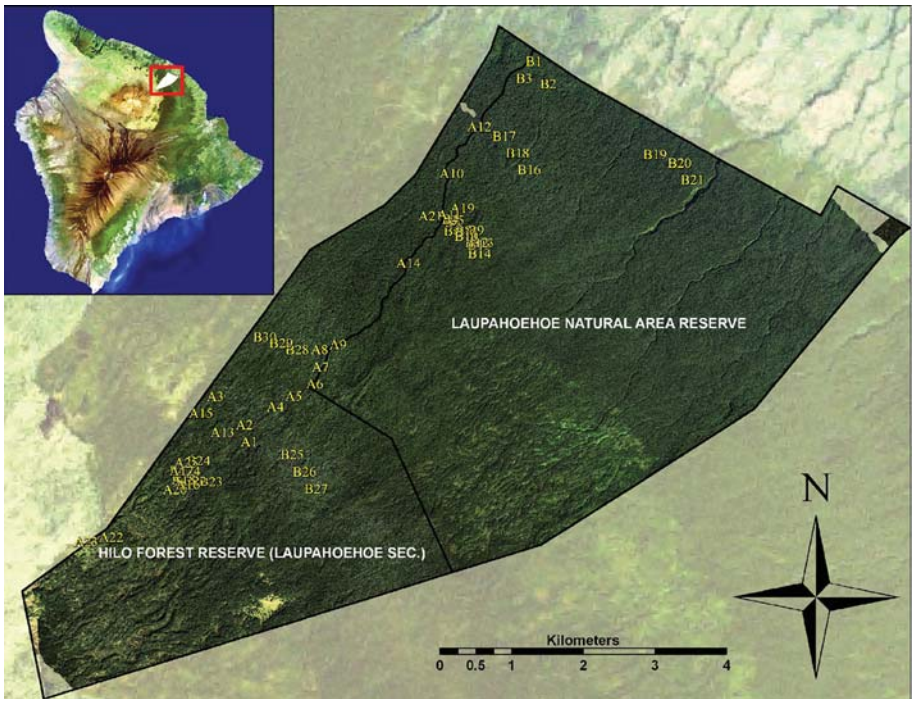


**Figure 1.** Natural color composite image of the study forest derived from Carnegie Airborne Observatory imagery. Field plots for aboveground biomass measurements are numbered in yellow. Inset shows location of the forest on the Island of Hawaii.

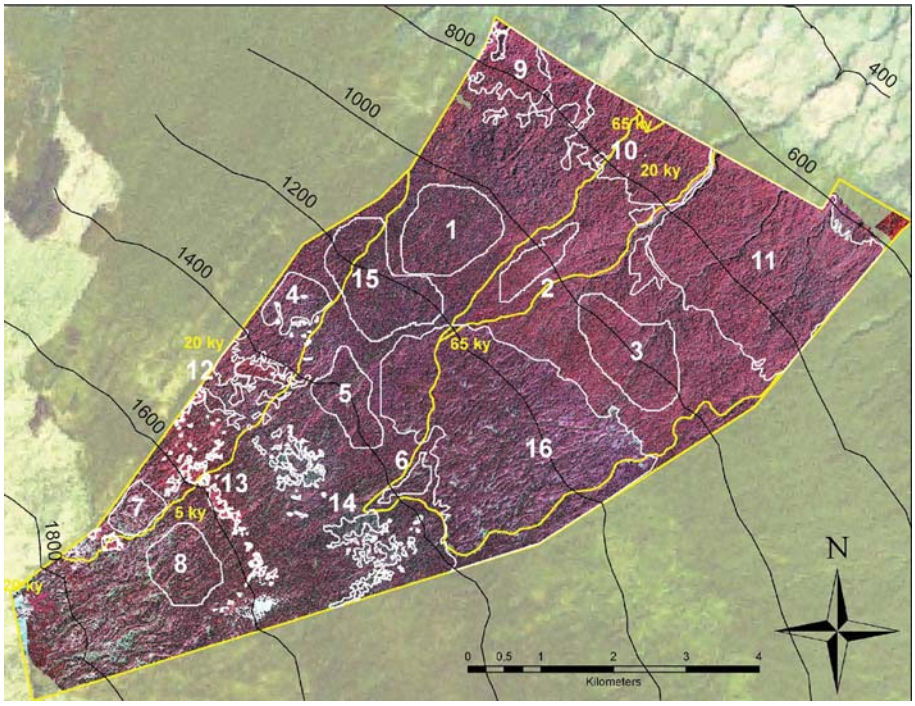


**Figure 2.** Color-infrared composition image of the study forest derived from Carnegie Airborne Observatory imagery, with polygons showing location of forests identified for landscape biomass analysis. Yellow delineates substrate age, and black lines indicate 200-m contour intervals.

## Remote Sensing System

Large-scale analysis of forest 3-D structure, canopy composition, and carbon stocks requires a combination of airborne technologies that simultaneously resolve the horizontal and vertical characteristics of the vegetation as well as the type of vegetation present. We used the Carnegie Airborne Observatory (CAO), a system designed to map the biochemical, taxonomic, and structural properties of vegetation and ecosystems (Asner and others 2007). The CAO combines three instrument sub-systems into a single airborne package: (i) High-fidelity Imaging Spectrometer (HiFIS); (ii) Light Detection and Ranging (lidar) scanner; and (iii) Global Positioning System-Inertial Measurement Unit (GPS-IMU). The CAO uses both in-flight and post-flight data fusion approaches to co-locate HiFIS and lidar data in 3-D space; this allows for automated ortho-geolocation of the combined HiFIS-lidar data stream.

## Data Collection and Analysis

In January 2007, we operated the CAO over the HETF, providing combined HiFIS and lidar measurements at approximately 1.25 m spatial resolution (ground sample distance; Figure 1). In previous work, the HiFIS data were calibrated, atmospherically corrected and classified to map the location of the dominant canopy species (native and invasive) (Asner and others 2008). Here, we utilized the information from the past spectral analysis, along with ground- and helicopter-based observations of the forest reserve, to develop polygons representing the major forest types shown in Figure 2, and listed in Table 1. The polygons were developed by both digital classification and manual interpretation, with buffer areas around the polygons of 100–300 m to maximize differences in composition, elevation (climate), substrate age, and relief. The focus here could then be placed on analysis of the lidar data with respect to vegetation dominance (native and invasive trees), substrate age, climate, and relief.

For this study, the CAO lidar was operated at 50 kHz, with a maximum half-scan angle of 17 (after 2-degree cutoff) degrees and 35–40% overlap between 19 adjacent flightlines. These adjacent flightlines ran along elevation contours, and sensor to target range was maintained at 2088 m with a standard deviation of 97 m throughout the data collection. This resulted in ±4.6% variation in laser ranging at the edge of each scan line, and ±6 cm variation in laser spot spacing. Laser spot size at ground level ranged from 1.21 to 1.33 m from nadir to the edge of each scan line (17° off-nadir).

The lidar point cloud data were analyzed in two steps: (i) a physical model was used to derive surface (top-of-canopy) and ground digital elevation models (DEM). Vegetation height was then esti-

**Table 1.** Characteristics of Major Vegetation-Terrain Combinations Found Throughout Study Region

| ID | Name | Canopy species[1] | Mean elevation (m) | MAP[2] (mm) | MAT[3] (C) | Substrate age (ky) | Analysis area (ha) |
|---|---|---|---|---|---|---|---|
| Substrate versus elevation among *M. polymorpha* stands | | | | | | | |
| 1 | Low-native | METPOL | 1094 | 4500 | 17 | 5 | 133 |
| 2 | Low-native | METPOL | 1018 | 4500 | 17 | 20 | 43 |
| 3 | Low-native | METPOL | 1002 | 4500 | 17 | 65 | 138 |
| 4 | Mid-native | METPOL | 1380 | 3500 | 15 | 5 | 44 |
| 5 | Mid-native | METPOL | 1320 | 3500 | 15 | 20 | 73 |
| 6 | Mid-native | METPOL | 1380 | 3700 | 15 | 65 | 17 |
| 7 | High-native | METPOL | 1673 | 2500 | 13 | 5 | 35 |
| 8 | High-native | METPOL | 1675 | 2500 | 13 | 20 | 82 |
| Forest composition—Species dominance, invasion, and dieback | | | | | | | |
| 9 | Low-invaded | PSICAT-FICRUB-METPOL | 802 | 4500 | 18 | 5 | 113 |
| 10 | Low-invaded | PSICAT-FICRUB-METPOL | 772 | 4500 | 18 | 20 | 193 |
| 11 | Low-invaded | PSICAT-FICRUB-METPOL | 755 | 4500 | 18 | 65 | 952 |
| 12 | *A. koa* | ACAKOA | 1457 | 3300 | 15 | 20 | 50 |
| 13 | *F. uhdei* | FRAUHD | 1614 | 2750 | 16 | 5, 20 | 32 |
| 14 | Dieback | METPOL | 1422 | 3750 | 14 | 5 | 61 |
| Relief | | | | | | | |
| 15 | Well drained | METPOL | 1212 | 4000 | 16 | 5, 20 | 191 |
| 16 | Poorly drained | METPOL | 1235 | 4000 | 16 | 65 | 747 |

[1]*Species abbreviations: PSICAT = Psidium cattleianum, FICMAC = Ficus rubiginosa, METPOL = Metrosideros polymorpha, FRAUHD = Fraxinus uhdei, ACAKOA = Acacia koa.*
[2]*MAP = mean annual precipitation.*
[3]*MAT = mean annual temperature.*

mated by differencing the surface and ground surface DEM (Lefsky and others 1999; Lefsky and others 2002b). Vertical errors in ground heights and vegetation heights were previously estimated to be 0.12 m (s.e. = 0.14 m) and 0.7 m (s.e. = 0.2 m), respectively, in a subset of the forest study that included both sloping and flat terrain, with and without tree cover (Asner and others 2007; Asner and others 2008). (ii) The large number of lidar points collected at high pulse rates made it desirable to represent the data in a more compact form for analysis of the vertical canopy structure. For this study, the vertical distribution of lidar points was calculated by binning them into volumetric pixels (voxels) of 5 × 5 m spatial resolution with 1 m vertical resolution. The DEM of ground elevation was used to standardize the vertical datum of each voxel. Therefore, the heights of each vertical ''slice'' of a vegetation canopy were defined relative to the ground at the horizontal center of each voxel. After the lidar points were binned in each volume cube, each vertical cube was divided by the total number of lidar points in that column, yielding the percentage of lidar points that occurred in each voxel. This approach has the positive effect of decreasing our sensitivity to localized variations in canopy leaf density or tree branch characteristics and flightline overlap pattern (major component of absolute variation), which can result in a different number of lidar returns from voxel to voxel.

## Field Measurements

The study area and field-based sampling extent are shown in Figure 1. Two independent teams of researchers were deployed to take field measurements between June and December 2007. At each site, the plot center was marked and a global positioning system (GPS) point taken with a survey-grade receiver (GS50 +, Leica Geosystems, St. Fallen, Switzerland). The GPS data were later differentially corrected using several available base stations. Each field team measured live trees using standard forestry tapes and equipment (for example, prisms). Group A sampled extensively but nonrandomly, in variably sized circular plots with 10–30 m radius (see Electronic Supplementary Material Appendix 1). Any stem or snag 5 cm diameter or greater at breast height (DBH) was measured, and all snags were considered live trees in subsequent biomass estimations. Group B utilized a stratified random sampling design, picking an arbitrary starting point at different elevations, and then measuring out three plots spaced 200 m apart

**Table 2.** Species-Specific Height-to-DBH Allometrics Used to Generate Plot-Level Estimates of Aboveground Biomass

| Species | Equation | $r^2$ | $n$ |
|---|---|---|---|
| *Acacia koa* | H = 6.1885 (ln DBH) − 5.6164 | 0.77 | 198 |
| *Fraxinus uhdei* | H = 8.853 (ln DBH) − 10.94 | 0.64 | 17 |
| *Ilex anomala* | H = 5.4902 (ln DBH) − 2.5559 | 0.90 | 17 |
| *Metrosideros polymorpha* | H = 5.6702 (ln DBH) − 4.0406 | 0.87 | 96 |
| *Psidium cattleianum* | H = 3.395 (ln DBH) + 1.3495 | 0.81 | 93 |
| Combined | H = 5.3595 (ln DBH) − 2.5581 | 0.82 | 421 |

*The equation for all data combined is also shown, and was used when other more scarcely abundant tree species were encountered in the plots. H = tree height; DBH = diameter at breast height. The data forming these equations are compiled from databases maintained at the Institute of Pacific Islands Forestry, US Forest Service, Hilo, Hawaii.*

and parallel to the elevation gradient. Circular plots with 24 m radii were intensively sampled for all snags and stems 5 cm or more DBH.

## Biomass Estimation

Chave and others (2005) have shown that allometric models utilizing a combination of DBH, height, and wood density measurements together are best for deriving AGB estimates in tropical forests. Although DBH and wood density are fairly easy to measure, the closed canopy and high basal area per ground area of this densely foliated tropical forest made height estimation very difficult with either analog or digital clinometers. As a compromise, we used species-specific allometric equations relating height (H) to DBH for the common canopy species found in this forest (Table 2). These equations were developed using common canopy species found across our entire forest site and other regions of Hawaii Island, and are maintained in a database by the Institute of Pacific Islands Forestry (US Forest Service, Hilo, HI) using an extensive array of field H and DBH measurements of trees commonly found in Hawaii. In addition, wood density values were derived from field-based wood samples and from the literature (Reyes and others 1992). We used the ''Wet Forest'' class from Chave and others (2005) to estimate biomass for each measured stem:

$$\mathrm{AGB} = 0.0776 \times \left(\rho D^2 H\right)^{0.94} \quad (1)$$

where AGB is estimated aboveground biomass in kg, ρ is wood density (g $cm^{-3}$), D is diameter at breast height (cm), and H is canopy height (m). Chave and others (2005) report a standard error of 12.5% and an $r^2 = 0.97$ for this equation. AGB values were derived for each species in each plot, summed, and then divided by the plot area to yield area-weighted biomass (Mg $ha^{-1}$).

## Lidar Height Indices

A proven approach to biomass estimation using airborne lidar is to apply regressions of lidar vertical profile indices to plot-based biomass estimates (Lefsky and others 1999, 2002a, b; Drake and others 2002, 2003; Popescu and others 2004). In this study, we tested a suite of lidar metrics: CH, canopy height squared (CH2), mean canopy height (MCH), and quadratic mean canopy height (QMCH)—the equations for MCH and QMCH can be found in Table 3, and are described by Lefsky and others (1999). We selected these particular metrics because they are readily calculated from voxelized lidar data and have proven sufficiently general for use with a variety of lidar sensors. Briefly, CH is the height of the tallest canopy element for a given set of lidar point cloud returns; here, it is the tallest point in each 5 × 5 m kernel. The CH2 is the squared value of CH. The MCH is the weighted height of the lidar point cloud in each 5 × 5 kernel (Table 3). The QMCH is similar but applies a greater weighting to upper canopy lidar points, thus biasing the presence of taller trees on the index. Whereas the CH and CH2 metrics rely only on height, the MCH and QMCH take into account the full vertical profile of the canopy.

We developed regressions between the lidar metrics and plot-level AGB estimates. Because the

**Table 3.** Vegetation Lidar Metrics Developed by Lefsky and Others (1999)

| | |
|---|---|
| Mean Canopy Height (MCH) | $=\sum_{i=1}^{h} \mathrm{CHP}(i) \times i$ |
| Quadratic Mean Canopy Height (QMCH) | $=\sqrt{\sum_{i=1}^{h} \mathrm{CHP}(i) \times i^2}$ |

*CHP = canopy height profile at each height (i) above ground to a maximum height (h).*

lidar resolution was much finer than the size of the field plots, we calculated three statistical measures of the lidar metrics—mean, median, and maximum—to compare to the biomass data. The twelve indices (4 lidar indices × 3 statistical measures) derived at each field plot were then regressed against the biomass value of that site, and the regression with the highest precision and lowest residuals was selected for subsequent spatial analyses of biomass stocks.

## Uncertainty Analysis

There are several known sources of uncertainty in developing field-based estimates of AGB in forest ecosystems (Clark 2002; Chave and others 2004). The uncertainties begin to compound with the measurement of individual tree DBH, height, and specific wood densities. There are additional errors associated with including or not including crown shape and diameter in the AGB estimates (Keller and others 2001; Palace and others 2008). These errors associated with the development of allometric equations have been the focus of many past studies, and the latest major synthesis of allometric equations for tropical forest species reports standard errors of just 5–12.5% (Chave and others 2005). However, there are also errors associated with geo-locating and co-locating remotely sensed and ground-based data. In particular, errors are generated by uncertainty in the location and number of trees found along plot edges that may or may not be included in the lidar analysis. From the remote sensing perspective, there are also uncertainties in the measurement of canopy height and 3-D vertical structure.

Here we assessed two specific remote sensing-related sources of uncertainty: (1) we quantified the compounded error caused by including/excluding trees from plots edges and co-location of plot centers and edges in the lidar data; and (2) we quantified the error caused by uncertainty in the lidar-AGB regressions. First, we determined uncertainty caused by variation in the estimated location and size of the field AGB plots. Each plot was offset by 10% of its nominal location in each of four diagonal directions. These four dislocations of the estimated plot location, along with the center, nominal location, gave a total of five plot location estimates. In addition, the plot size was increased and decreased by 10% in area. This variation, along with its nominal size, gave a total of three different plot sizes. By iterating the lidar vertical profile metrics for each of these cases, we generated a distribution of 15 values for each plot. The standard deviation of this distribution was divided by the square root of the sample size ($n$ = 15) to get an estimate of the standard error.

Next, using the field data from sample plots, the mean and median values of the lidar metrics were regressed separately against AGB to generate linear and quadratic equations. The standard error of the estimate was used to create a prediction confidence interval using the formula:

$$\text{Interval} = t_{\text{critical}} \times Y_{\text{se}} \times \text{sqrt}\left(1 + 1/n + \left((x_{\text{new}} - x_{\text{mean}})^2\right)/X_{\text{ss}}\right) \quad (2)$$

where:

$t_{\text{critical}}$ = the critical $t$ value for a given level of confidence

$Y_{\text{se}}$ = the standard error for the dependent variable (standard error of the estimate)

$x_{\text{new}}$ = the new independent variable from which a prediction of $y$ will be made

$x_{\text{mean}}$ = the average of the × values used to create the regression

$n$ = the number of samples

$X_{\text{ss}}$ = the sum of the squared x's.

This interval value (plus or minus) represents the uncertainty in the remotely sensed AGB prediction.

## Statistical Analyses

Following the mapping steps outlined above, we analyzed the resulting forest structure and AGB maps in relation to environmental controls and canopy dominance (Table 1; Figure 2). All structural comparisons used a random selection of 50,000 5 × 5 m lidar vertical profile kernels. The biomass comparisons were carried out after resampling the AGB map to 33 × 33 m (0.1 ha) resolution, which simulated a typical biomass plot used in many tropical forest studies (Phillips and others 1998). Following resampling, 150 of these 0.1 ha kernels were randomly selected within each forest type for comparison. The 50,000 and 150 sample sizes were set to accommodate the smallest forest type included in the comparisons (vegetation type 1, 17 ha; Table 1). These random selection procedures ensured that statistical comparisons had balanced sample sizes, and that spatial autocorrelation was minimized. Distributions of AGB values for each forest type were compared using Kolmogorov–Smirnov (K–S) tests.

# Results

## Field Measurements

The summary of field measurement results for each of the 58 plots is provided in Electronic Supple-

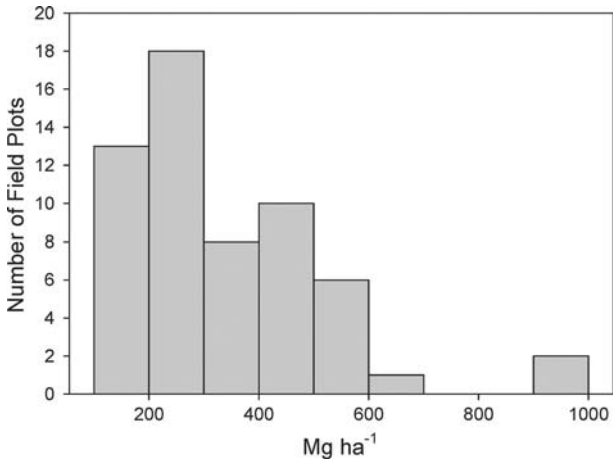


**Figure 3.** Distribution of aboveground biomass among 58 field plots used for subsequent lidar analyses.

mentary Material Appendix 1, and a histogram of the estimated plot-level AGB is shown in Figure 3. Mean (±s.d.) of AGB was 341.8 (179.3) Mg ha$^{-1}$, with a range of 123.1–958.9 Mg ha$^{-1}$ (see Electronic Supplementary Material Appendix 1). The median AGB value was 282.6 Mg ha$^{-1}$, with a non-normal distribution and a skewness of 1.40 (Figure 3).

## Forest Structure

The lidar canopy profiling results were compiled by forest type (Table 1) to develop vertical profile statistics for each native *M. polymorpha* stand (Figure 4). In this section, all noted differences in vertical layering, as defined by the number of lidar returns counted between discrete minima in the vertical strata (Asner and others 2008), were statistically significant (*t*-tests; $P < 0.05$). All stands had a clearly delineated understory vegetation layer 0–1 m tall. Each forest also had a well defined mid-canopy layer which varied in height above the ground. The lowland native forests had mid-canopy layers ranging from 4.8 (±1.3) m height on 5 ky old substrate, to 8.2 (±1.6) m on 65 ky substrates (Figure 4A). The tallest lowland forest canopies reached 37.5, 30.5, and 32.5 m on 5, 20, and 65 ky substrates, respectively. However, only the 5 ky stand was statistically taller than the 20 ky or 65 ky stands (*t*-tests; $P < 0.05$). Among lowland *M. polymorpha* stands, overstory canopy volumes also varied by substrate age (Figure 4A). The partitioning of canopy volume on 5 ky substrates was 45, 23, and 32% for strata in the 0–10 m, 10–20 m, and 20 + m height classes, respectively. In contrast, the 65 ky substrates supported native forest vol-

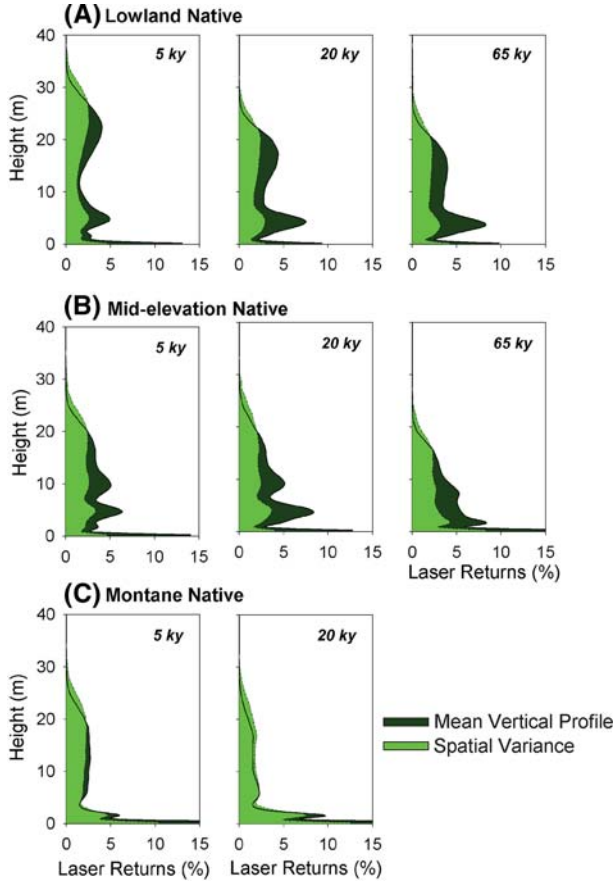


**Figure 4.** Vertical canopy profile statistics of the native *M. polymorpha* forest landscapes across substrate age and elevation gradients.

umes of 58, 36, and just 6% in the same three vertical strata (Figure 4A).

At mid-elevation, *M. polymorpha*-dominated stands reached a maximum height of approximately 33 m on 5 ky and 20 ky substrates, whereas they never exceeded 26 m on the oldest 65 ky surfaces (Figure 4B). The mid-canopy stratum was bi-modal in all three of these forest stands, with peak volumes ranging from 2 to 5 m in the lower vertical layer and 8–10 m in the upper layer. At mid-elevation, the 65 ky substrates had the shortest *M. polymorpha* canopies with more volume partitioned in the lowest vertical layers. All three of these mid-elevation stands partitioned more canopy volume in the 0–10 m and 10–20 m strata (Figure 4B) in comparison to the lowland stands that supported more canopy volume in the 20–30 m range (Figure 4A).

In the montane reaches of the forest, the *M. polymorpha* canopy opened laterally, resulting in large spatial variation in canopy vertical profiles (Figure 4C). Here, 68 and 82% of the canopy vol-

ume was contained in the 0–10 m layer for stands on 5 ky and 20 ky substrates, respectively. The 5 ky forest maintained nearly twice the canopy volume in the 10–20 m height range as that of the 20 ky stands, but neither forest exceeded 31 m in height (Figure 4C).

The lowland forest stands containing more than 50% cover of invasive *P. cattleianum* and *F. rubiginosa* had vertical canopy profiles (Figure 5A) that differed markedly from those of neighboring native *M. polymorpha*-dominated stands (Figure 4A). The 0–10 m height range contained 58, 65, and 67% of the measured canopy volume for invaded forests on 5, 20, and 65 ky substrates, respectively. The mid-canopy 10–20 m stratum contained most of the remaining canopy volume (28–34%), independent of substrate age. Although maximum tree heights were 38–45 m in the invasion zone, volumetrically, these tall trees contributed far less than 1% to the total forest volume (Figure 5A).

Forest stands dominated by specific species, including *F. uhdei* and *A. koa*, had contrasting vertical profile statistics, with the former species maintaining 48% of its volume above 20 m height

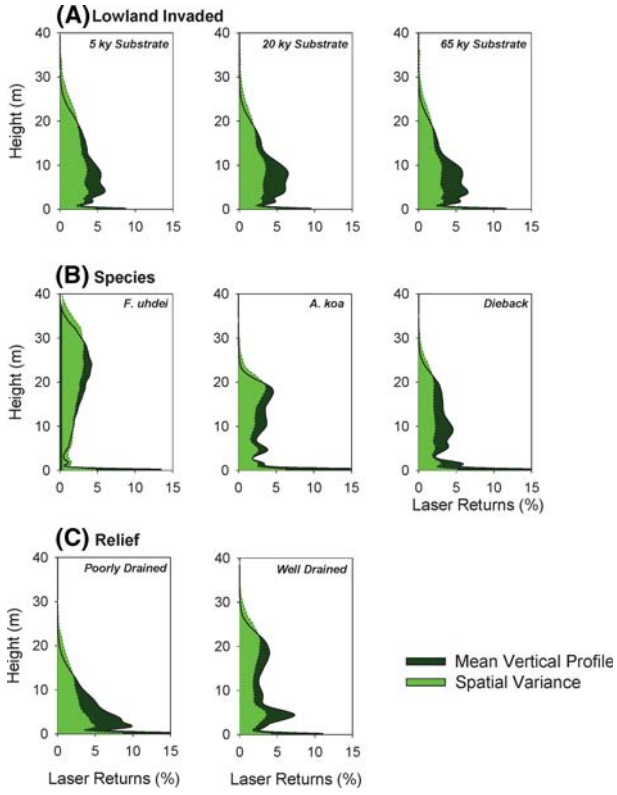


**Figure 5.** Vertical canopy profile statistics of the (**A**) lowland invaded stands across substrate ages; (**B**) stands dominated by invasive *F. uhdei*, native *A. koa*, or *M. polymorpha* dieback; and (**C**) stands on contrasting relief.

and the latter filling 39% of the forest layer between 10 and 20 m (Figure 5B). The tallest *F. uhdei* canopy was detected at 43.5 m, whereas the tallest *A. koa* was limited to 32.5 m in height. Canopies of *M. polymorpha* dieback, where the trees are dead but still standing (Mueller-Dombois 1987), covered about 131 ha, and reached heights of 32.5 m (Figure 5B). Dieback canopies maintained volumes of 59, 33 and 8% in 0–10 m, 10–20 m, and 20 + m layers, respectively. The lowest layers were dominated by shorter live vegetation, which could be viewed in close-ups of the CAO spectrometer data.

A change in relief that causes persistent bog-like conditions between 1100 m and 1400 m elevation (Figure 2; Table 1) resulted in canopy structural properties that differed from canopies on well-drained relief at the same elevation (Figure 5C). The poorly drained area maintained 84% of its canopy volume in the 0–10 m height range, with less than 1% of the canopy exceeding 17 m. In contrast, the well-drained forested area maintained a three-layer canopy exceeding 32 m in height (Figure 5C). However, most of the canopy volume was still contained in the 0–10 m (53%) and 10–20 m (32%) strata.

It is important to note that the vertical profiling results described above are, to some degree, particular to our lidar sensor configuration (described in the Methods) and the electro-optical capabilities of the sensor. Comparison of lidar profiles on a laser shot-by-shot basis can become problematic if the instrument dead-time, which is the minimum vertical distance required for two objects to be distinctly detected, is too long (Morsdorf and others 2006). Our instrument dead-times are approximately 1 m in vertical distance, therefore the statistical comparisons presented above were limited to major variations in canopy vertical stratification extending over many meters of distance. In addition, we limited our interpretation of these vertical strata to large ($n$ = 150,000) sample sizes, which diminished our sensitivity to localized uncertainties caused by laser dead-time. In a study of vegetation structure in similar Hawaiian forests, Asner and others (2008) were able to validate this approach to estimating vertical structural variability and understory plant cover at the ecosystem level.

## Aboveground Biomass

All of the lidar metrics we tested were significantly correlated with field-estimated AGB (Figure 6). The best relationships were found using mean MCH and QMCH methods with linear regression ($r^2$ = 0.78 and 0.76; $P < 0.0001$):

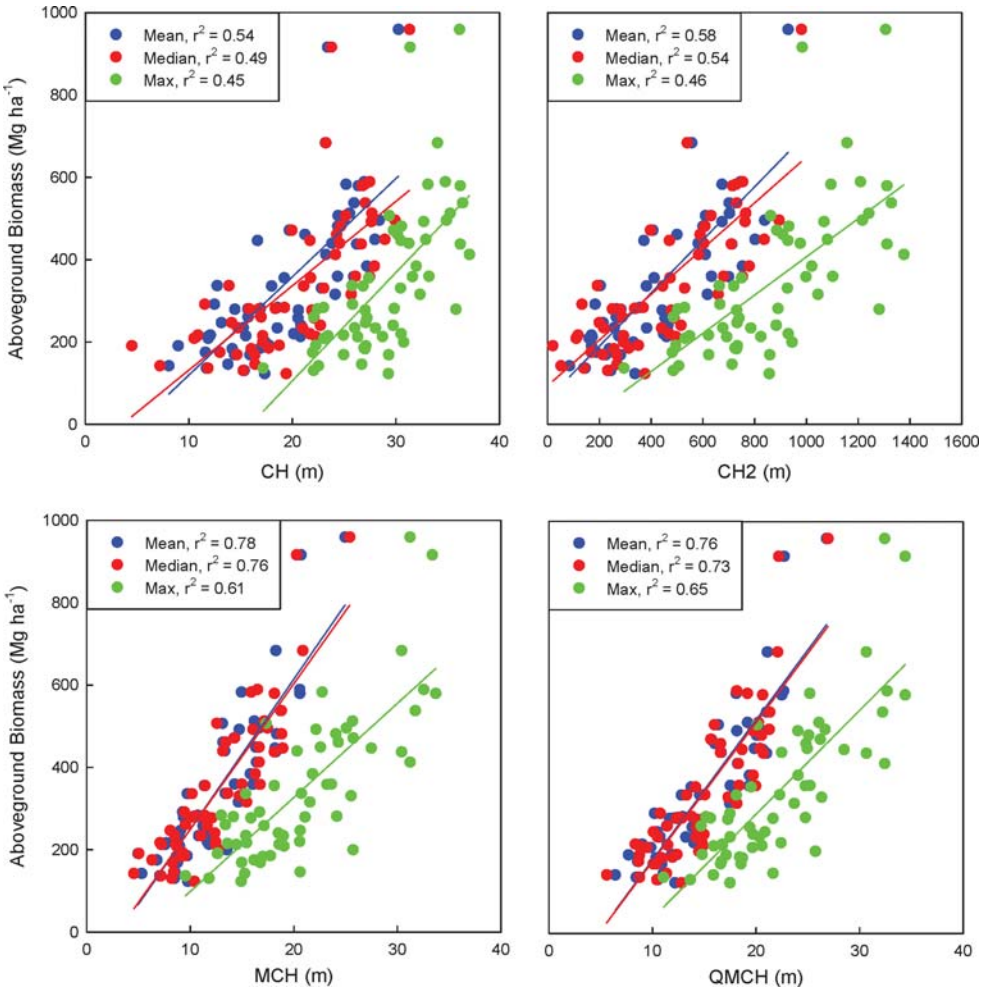


**Figure 6.** Relationships between field-estimated aboveground biomass and 12 airborne lidar metrics: the mean, median, and maximum values of canopy height (CH), canopy height squared (CH2), mean canopy height (MCH), and quadratic mean canopy height (QMCH; Lefsky and others 1999).

$$\mathrm{AGB} = -114.66 + 36.43(\mathrm{MCH}_{\mathrm{mean}}) \qquad (3)$$

$$\mathrm{AGB} = -162.02 + 34.01(\mathrm{QMCH}_{\mathrm{mean}})$$

Therefore, we employed the equation using the MCH metric to estimate AGB throughout the study area. When applying this equation to the lidar data, we set the biomass values to zero when the MCH was less than 3.14 m, which is the weighted vertical profile height at which equation (3) becomes negative. This cut-off represents the lower detection limit for this particular allometric equation relating the lidar data to aboveground biomass.

The resulting aboveground biomass map is shown in Figure 7. The highest biomass levels exceeding 500 Mg ha$^{-1}$ were found in the lowland native *M. polymorpha* stands and the higher elevation *F. uhdei* stand. The lowest AGB levels were mapped on the poorly drained relief as well as in herbaceous interspaces between tree canopies at very high elevations (≥1700 m). Among stands dominated by native *M. polymorpha* trees, there was an observable gradient of decreasing AGB as elevation increased (black arrow, Figure 7). Aside from this gradient, the *F. uhdei* stand, and the major relief change (bog), most other localized variations in AGB appeared to be related to small-scale relief changes including riparian zones. In the northeast lowland portion of the reserve, however, AGB levels declined in areas most heavily infested with the invasive trees *P. cattleianum* and *F. rubiginosa* (comparing Figures 2 and 7).

Uncertainty analyses indicated that AGB estimation errors caused by misalignment of lidar and field data were small, ranging from 0 to 10 Mg ha$^{-1}$ (Figure 8A). The distribution of this co-location uncertainty was highly skewed (Figure 9A), with 80% of the values falling in the 0–4 Mg ha$^{-1}$ range. In contrast, the mapping uncertainty caused by the plot-based AGB estimates, which incorporate all of the compounded errors due to worker bias, height-to-DBH allometrics (Table 2), and the applied AGB

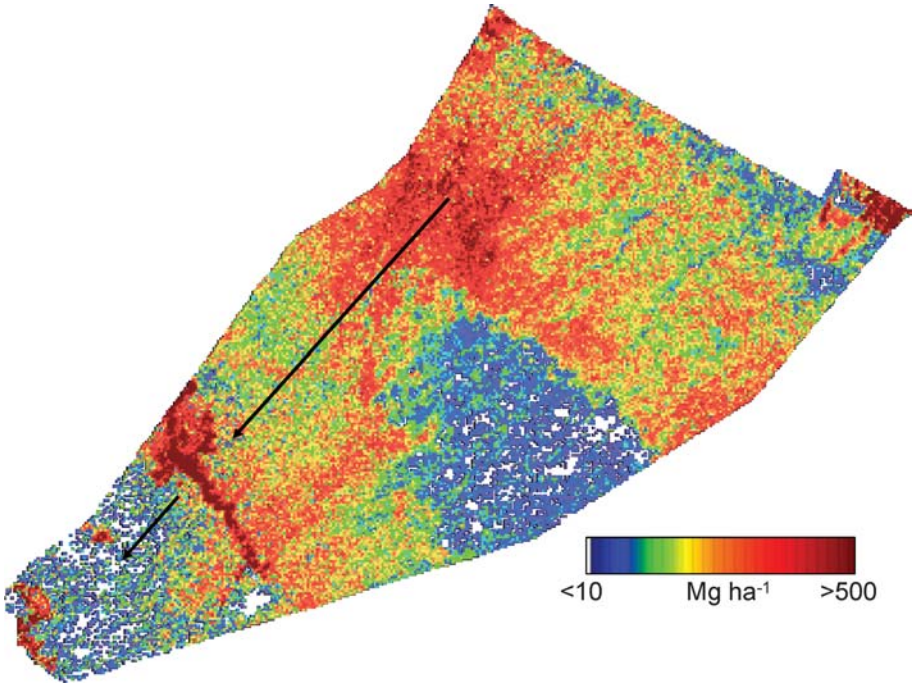


**Figure 7.** Aboveground tree biomass (AGB) estimated at 0.1 ha resolution using the LiDAR data. The black arrow highlights a gradient of decreasing AGB with increasing elevation among stands dominated by native *M. polymorpha* trees.

equation from Chave and others (2005) were nearly constant (Figure 8B). Here, the mapping uncertainty ranged from 78 to 90 Mg ha$^{-1}$, with more than 90% of the uncertainty holding constant at about 80–82 Mg ha$^{-1}$ (Figure 9B). Slightly higher uncertainties reaching 86–90 Mg ha$^{-1}$ occurred in areas with little tree cover (high-elevation woodland/grassland area, bog area) (Figure 8B).

## Environmental Controls

Analysis of native *M. polymorpha* forests indicated that the highest average AGB levels were 362.8 (±69.5) Mg ha$^{-1}$ in lowland stands on 5 ky substrate, and the lowest values of 47.7 (±55.7) Mg ha$^{-1}$ were found in the montane site on 20 ky substrates (Table 4). Maximum AGB values were 545 Mg ha$^{-1}$ in the lowland stand on 5 ky substrates, whereas the maximum values were constrained to only 206 and 246 Mg ha$^{-1}$ at mid-elevation/65 ky and montane/20 ky sites, respectively.

Across substrate ages of 5–65 + ky, AGB decreased significantly by 42% and 53% at lowland and mid-elevation, respectively (*t*-tests; $P < 0.01$). In the montane region, AGB declined 23% when going from the 5–20 ky substrates (*t*-test; $P < 0.01$). With increasing elevation that represented a precipitation and temperature decrease of >1500 mm y$^{-1}$ and 5°C, respectively, biomass levels decreased by 64% on the 5 ky and 82% on the 20 ky substrates (Table 4; *t*-tests $P < 0.001$). On 65 ky substrates found only at low- and mid-elevation, AGB decreased by 53% as elevation increased ($P < 0.01$).

Variation in AGB was evident in histograms developed from a random 150 point (150 × 0.1 ha) sampling of each forest stand (Figure 10). Biomass in lowland and mid-elevation stands was nearly normally distributed, whereas the distributions were skewed in the montane stands. Within each elevation zone as well as within each substrate-age class, all distributions of AGB were statistically different (Kolmogorov–Smirnov tests; *p*-values ranging from <0.001 to 0.02). The coefficient of variation (CV) of AGB was 19.2–23.3% among the lowland stands on different substrate ages. The CVs increased to 27.9–48.3% among mid-elevation stands, and was maximal in the montane stands on the two substrates (CV = 65% on 5 ky substrate; 117% on 65 ky substrate).

## Biological Invasion

In lowland stands, areas now heavily invaded by *P. cattleianum* and *F. rubiginosa* maintained AGB levels averaging 225.0 (±92.2), 192.1 (±71.0) and 172.3 (±67.8) Mg ha$^{-1}$ on 5, 20, and 65 ky substrates, respectively (Table 4). All of these invaded stands harbored significantly lower biomass levels in comparison to their native-dominated counterparts (*t*-tests; $P < 0.001$–0.05). The spatial distributions

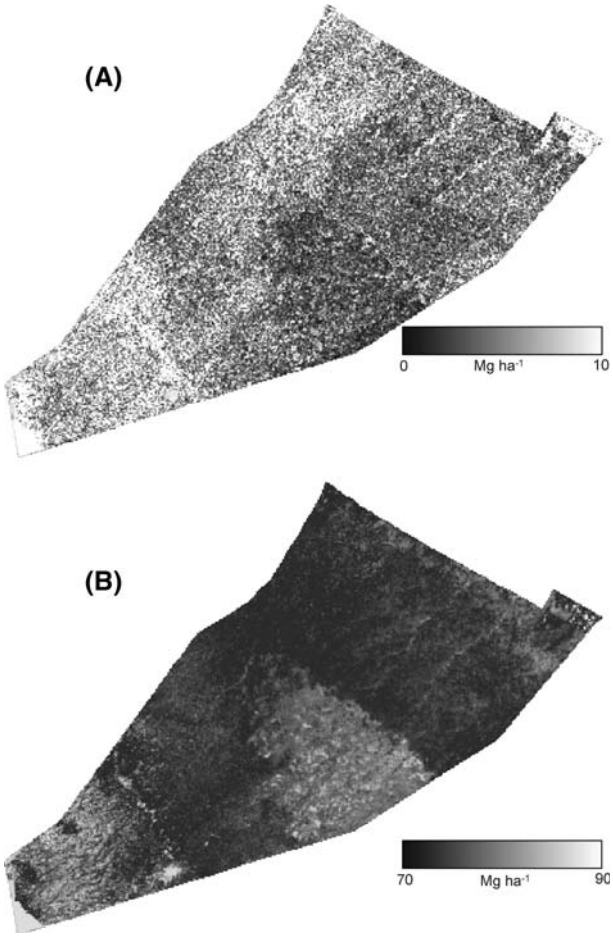


Figure 8. **A** Uncertainty in biomass estimates based on field plot size and location; **B** Uncertainty in biomass estimates based on field-based biomass estimates in relation to airborne lidar metrics.

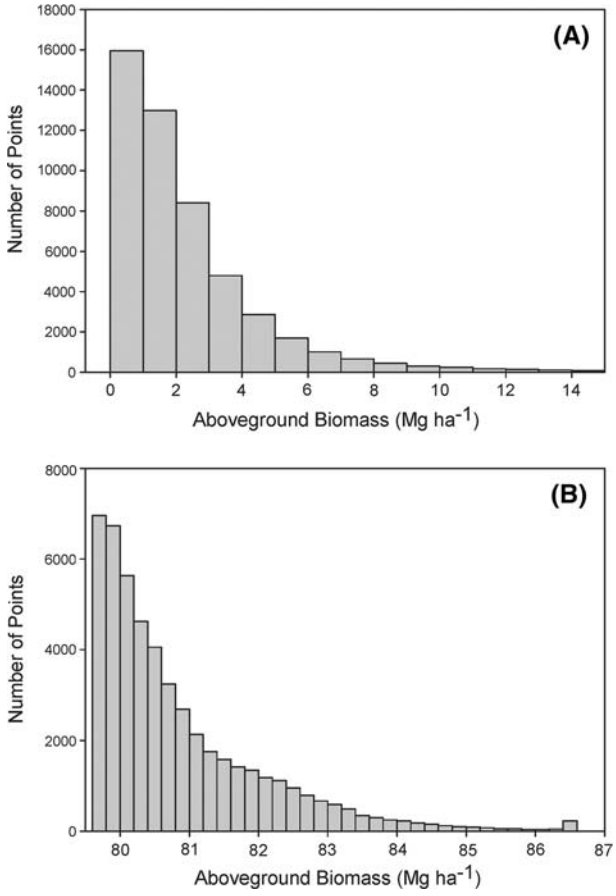


Figure 9. **A** Distribution of the uncertainty in aboveground biomass caused by field plot-to-lidar co-location error. **B** Distribution of the uncertainty in aboveground biomass caused by uncertainty in field biomass measurements as related to the airborne lidar data.

of AGB within the invasion zone were unique on each substrate age (Figure 11; K–S tests; $P < 0.05$) as well as in comparison to native stands (Figure 10; K–S tests; $P < 0.001$). Coefficients of variation in AGB were about twice as high in the invaded lowland stands (37–41%) than they were in the native lowland stands (19–23%). Dominance by the introduced *F. uhdei* tree resulted in high AGB levels of 508.5 (±167.4) Mg ha$^{-1}$, with a maximum estimated value of 834.6 Mg ha$^{-1}$ in one particular location (Table 4).

## Other Sources of Biomass Variation

The native nitrogen-fixing *A. koa* maintained AGB values of just 199.3 (±57.6) Mg ha$^{-1}$, but nonetheless could reach levels as high as 339.1 Mg ha$^{-1}$—a value nearly matching that of neighboring *M. polymorpha* stands. The *M. polymorpha* dieback area on 5 ky substrate (Figure 2) had AGB levels of 192.1 (±53.5) Mg ha$^{-1}$, with a maximum recorded value of 364.1 Mg ha$^{-1}$ (Table 4). These values fell between those of the mid-elevation and montane live *M. polymorpha* stands on the same substrate age. The AGB distributions of these three types of canopy dominance were each significantly different (Figure 11; K–S tests; $P < 0.05$).

Large-scale variation in relief leading to poor drainage resulted in suppressed biomass levels of 65.8 (±51.9) Mg ha$^{-1}$ (Table 4). The high variation in the bog forest (CV = 79%) was related to the skewed distribution of the results (Figure 11), which was significantly different from that of the adjacent forest stands on well-drained relief (K–S test; $P < 0.0001$). The well-drained area maintained AGB levels of 275.4 (±79.4) Mg ha$^{-1}$ (max. value = 436.1 Mg ha$^{-1}$), which placed its values between those of the lowland and mid-elevation *M. polymorpha* stands (Table 4).

**Table 4.** Aboveground Tree Biomass (Mg ha$^{-1}$) Statistics of Major Forest Types Considered in This Study

| Name | Substrate age (ky) | Mean | Median | Standard deviation | Maximum |
|---|---|---|---|---|---|
| Substrate versus elevation among *M. polymorpha* stands | | | | | |
| Low-native | 5 | 362.8 | 358.2 | 69.5 | 545.0 |
| Low-native | 20 | 254.2 | 257.3 | 52.0 | 380.2 |
| Low-native | 65 | 211.7 | 212.3 | 49.4 | 346.1 |
| Mid-native | 5 | 213.3 | 210.8 | 59.5 | 397.5 |
| Mid-native | 20 | 182.0 | 177.3 | 55.0 | 374.2 |
| Mid-native | 65 | 99.2 | 106.7 | 47.9 | 205.7 |
| High-native | 5 | 130.7 | 114.7 | 85.0 | 342.5 |
| High-native | 20 | 47.7 | 26.7 | 55.7 | 246.1 |
| Forest composition—species dominance, invasion, and dieback | | | | | |
| Low-invaded | 5 | 225.0 | 217.1 | 92.2 | 608.6 |
| Low-invaded | 20 | 192.1 | 195.5 | 71.0 | 365.8 |
| Low-invaded | 65 | 172.3 | 168.1 | 67.8 | 340.2 |
| *A. koa* | 20 | 199.3 | 207.8 | 57.6 | 339.1 |
| *F. uhdei* | 5, 20 | 508.5 | 529.8 | 167.4 | 834.6 |
| Dieback | 5 | 192.1 | 189.9 | 53.5 | 364.1 |
| Relief | | | | | |
| Well drained | 5, 20 | 275.4 | 277.7 | 79.4 | 436.1 |
| Poorly drained | 65 | 65.8 | 66.9 | 51.9 | 282.4 |

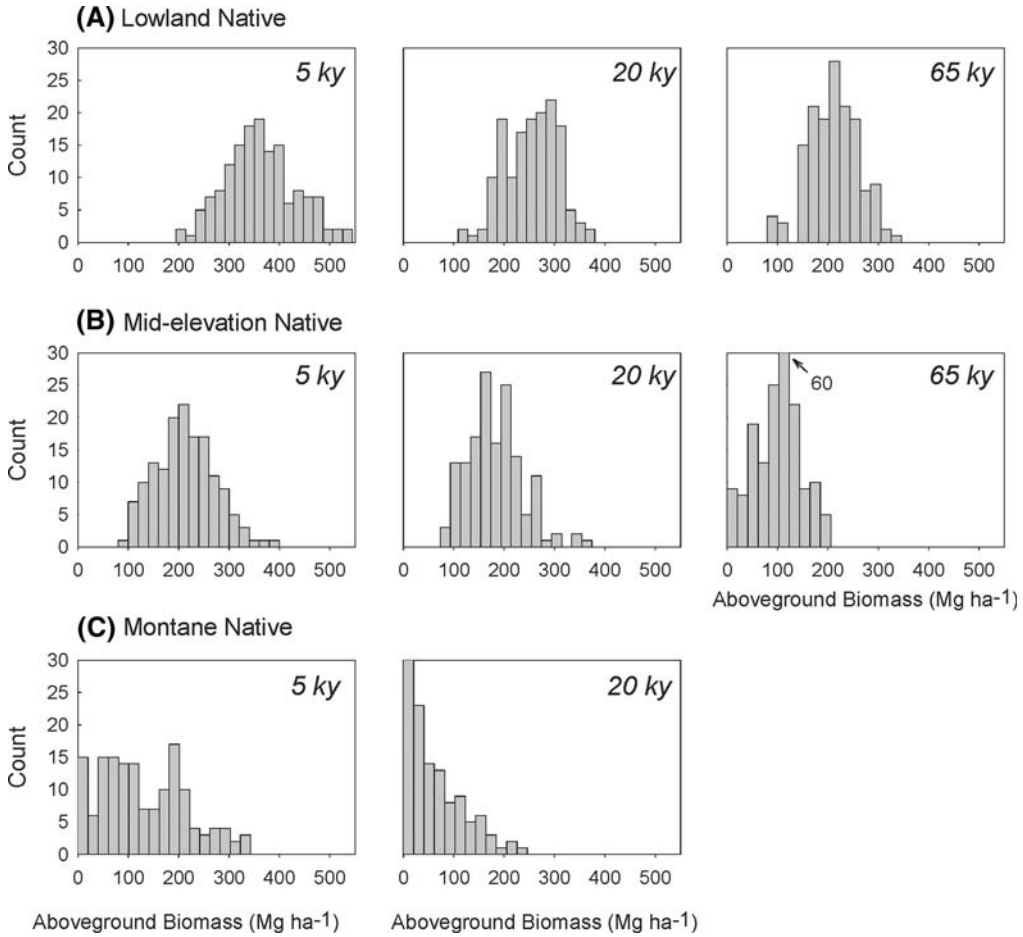


**Figure 10.** Histograms of aboveground tree biomass for native *M. polymorpha* forests on three substrate ages and in three elevation zones.

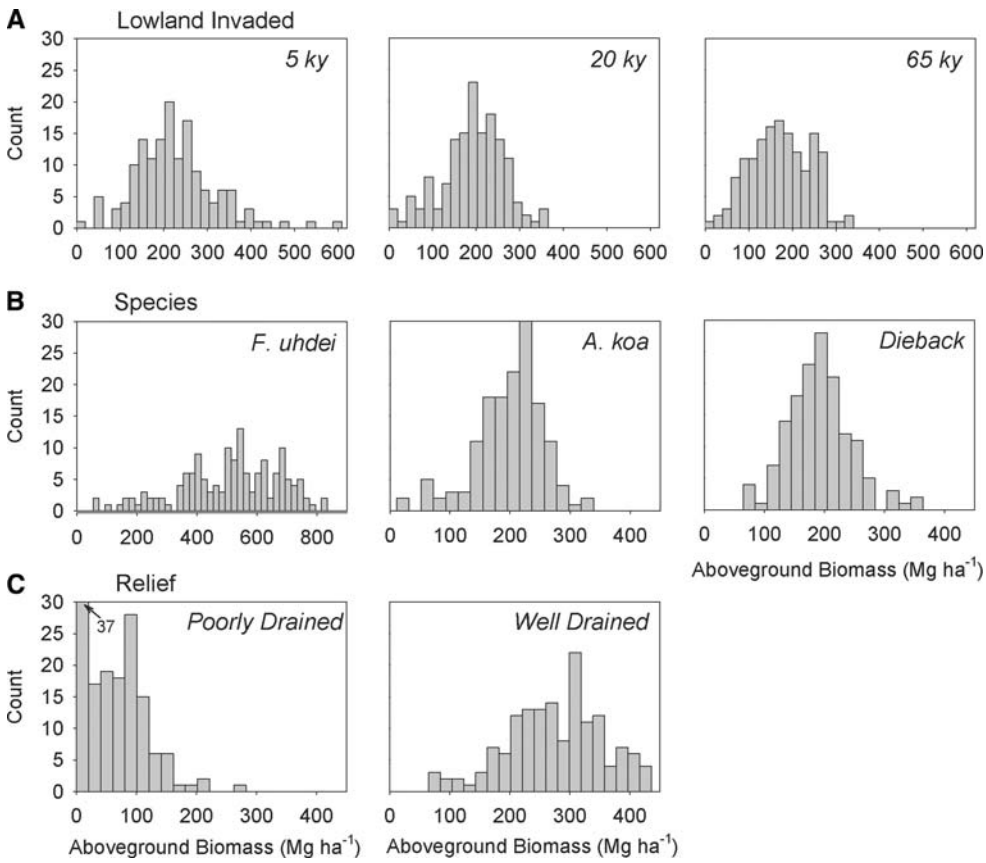


**Figure 11.** Histograms of aboveground tree biomass for: **A** forests on different substrates that are invaded by *P. cattleianum* and *F. rubiginosa*; **B** forests invaded by non-native *F. uhdei* or dominated by either native *A. koa* or dieback of *M. polymorpha*; **C** native forest on poorly drained and well-drained relief.

## Discussion

### Sources of Biomass Variation

Our results show clear patterns in AGB variation corresponding to precipitation and temperature (increasing elevation), substrate age (5–65 ky), species dominance, and at least one major change in topographic relief across this rain forest landscape. Among native *M. polymorpha* stands, the highest AGB levels were measured in the warmest, wettest conditions on the youngest (5 ky) substrate (Figure 10). Biomass declined in cooler/drier conditions and on older substrates. Both the mean AGB levels and their distributions changed significantly across this matrix of conditions.

In this region of Hawaii Island, where soils are more fertile than on younger (for example, Kilauea and Mauna Loa volcanoes) and older (for example, Kauai) substrates (Vitousek 2004), we found that AGB of native forest is more closely tied to climate than to substrate age. Specifically, our airborne estimates indicated a 23–53% decline in AGB with increasing substrate age, with the largest decreases at higher elevation. Increasing elevation corresponded to a 53–84% decline in AGB, with the largest decreases on older substrates. Plot-level measurements by Raich and others (1997) suggested that AGB decreased only 34% across a similar elevation range on Mauna Loa Volcano, but these changes were measured on 0.1 ky substrates. Aplet and Vitousek (1994) measured AGB on substrates from 0–3.4 ky at elevations from 914 to 2,438 m, and found the highest biomass levels on oldest substrates at the lowest elevation. Plot studies crossing a long substrate-age gradient of 0.3, 20, 150, and 4100 ky indicated maximum canopy heights and biomass levels on 20 ky old soils (Vitousek 2004). Our airborne estimates indicated a similar decline in biomass after 20 ky, but our peak biomass was measured at 5 ky, which is more in line with the results from Aplet and Vitousek (1994). These findings suggest that, in terms of carbon storage, the long-term decline occurs relatively early in Hawaiian substrate chronosequences.

Spatial variation in the biomass of native forest stands also changed with elevation and substrate age. AGB variation was lowest on the 5 ky substrates in lowland forests (CV = 19.2%), and highest in the montane, native stands on 20 ky substrates (CV = 116.8%). Spatial variation was far more sensitive to elevation (for example, 6-fold increase on 20 ky substrates) than to substrate age at constant elevation (for example, 2-fold increases

at mid-elevation and in the montane). The heightened biomass variability with elevation suggests that the establishment and growth of native tree species is limited by climate constraints on their physiology and/or reproduction (Raich and others 1997; Cordell and others 1998; Raich and others 2006).

Biological invasion had a profound effect on the structure and biomass of the rain forests we studied. Most notably, we found that the proliferation of two highly invasive tree species—*P. cattleianum* and *F. rubiginosa*—into lowland stands corresponds to decreased AGB (Table 4). This invasion-mediated decline in biomass contrasts with some previous studies which find that invasion increases AGB (Ehrenfeld 2003), although Bhatt and others (1994) also documented biomass declines when Himalayan forests were invaded and replaced by the alien shrub, *Lantana camara*. Moreover, our airborne measurements indicated a 38, 24, and 19% decrease in AGB following invasion on 5, 20, and 65 ky substrates, respectively. That is, there is a substrate-age dependence of biomass change following invasion. This occurred because, despite a strong substrate-age control on native forest biomass (212–368 Mg ha$^{-1}$), there was nearly constant biomass following invasion (172–225 Mg ha$^{-1}$), implying that although native forest biomass is significantly influenced by soil age, invaded forest biomass is not, at least in these landscapes.

Our interpretation of how this invasion has affected AGB levels assumes that the invasion is fairly mature. Although we could not fully test this assumption, our field measurements (see Electronic Supplementary Material Appendix 1) indicate size classes among the invaders that would make their presence decades old (Huenneke and Vitousek 1990; Asner and others 2008). Furthermore, historical records suggest that the invasion was well established by the 1970 s or even earlier (DLNR 1989). In sum, we believe that this biological invasion is reducing aboveground carbon stocks in these lowland forest stands, a process we observed as canopy structural changes in other Hawaiian forests following the spread of *P. cattleianum* (Asner and others 2008). Similarly, in lowland forest remnants of the Puna District on Hawaii Island, Zimmerman and others (2007) found that, although overall basal area was dominated by large remnant *M. polymorpha* individuals, stem densities were dominated by mid-canopy stands of *P. cattleianum*. The authors suggested that these forests will eventually lose the native overstory biomass as *M. polymorpha* individuals senesce and are replaced by monotypic stands of *P. cattleianum*.

In contrast to the lowland forest invasion results, the establishment of alien *F. uhdei* has caused a 7- to 10-fold increase in AGB in the montane portion of the forest reserve (Table 4). We observed the highest biomass levels within a core area along a road where this species was planted in the late 19th century (Figure 7). The species started as a forestry experiment that included the removal of native plants, but the experiment was later abandoned citing poor wood properties (Carlson and Bryan 1963; Francis 1990). Our lidar mapping showed that AGB was lower along the edge of the planted stand, where the species is now thought to be slowly expanding its range both uphill and downhill from the planting road (Rothstein and others 2004). In these areas of spreading trees, AGB ranged from about 174–349 Mg ha$^{-1}$, which was lower than the core planted area where biomass levels reached 835 Mg ha$^{-1}$.

These results suggest that *F. uhdei* is a carbon sink on a per hectare basis in the montane reaches of the reserve, which contrasts with the measureable carbon loss associated with *P. cattleianum*/*F. rubiginosa* proliferation in the lowlands. It thus appears that carbon storage may be enhanced or diminished by invasion, and that the direction and magnitude of biomass change depends upon the particular invasive species and the background environmental conditions. In Hawaii, many protected rain forest (and other) reserves have been and continue to be overtaken by alien plant species, most with yet unmeasured changes in carbon storage. To our knowledge, these are the first landscape-level estimates of whether invasive tree species alter carbon stocks across a tropical forest landscape in Hawaii or anywhere. It is therefore not yet possible to generalize the relative importance of biotic (for example invader lifeform or life strategy) or environmental (climate, soils) controls determining whether a system will become a carbon source or sink following invasion. Additional species, ecosystems and environmental settings need to be considered before we will understand the broad patterns of carbon-storage response to invasion.

Although forest areas dominated by native *A. koa* or *M. polymorpha*-dieback did not correspond to changes in AGB, neighboring variation in topographic relief had enormous effects on carbon stocks (Table 4). We measured a 76% lower average AGB on the poorly drained, bog terrain in comparison to the neighboring well-drained relief. In the bog forest, maximum biomass levels reached just 282 Mg ha$^{-1}$, a value roughly two-thirds of that found on well-drained relief at the same ele-

vation. However, the spatial variation in AGB was nearly three times higher in the bog area (Figure 7), owing to the highly localized affects of this large terrain feature on the landscape. Beyond these broad terrain effects, inspection of our AGB map (Figure 7) clearly indicates that local-scale variation in relief, ranging from dissected streams to raised hills, impart a pattern in biomass levels.

## Estimating Aboveground Biomass

Our mean AGB estimates for the rain forests of Laupahoehoe ranged from 47.7 Mg $ha^{-1}$ in native montane stands to 508.5 Mg $ha^{-1}$ (max = 834.6) in non-native, montane stands (Table 4), representing a nearly global range of values for tropical forests (Brown and Lugo 1984; Houghton and others 2000). How reliable are our estimates? On the one hand, this 10-fold biomass variation among forest types was far larger than the uncertainties (~80 Mg $ha^{-1}$) in our airborne mapping approach (Figure 9). On the other hand, the standard deviation of estimated AGB within a forest type ranged from 47.9 to 92.2 Mg $ha^{-1}$, with a uniquely high value of 167.4 Mg $ha^{-1}$ in the *F. uhdei* stand. Hence, our 80 Mg $ha^{-1}$ uncertainty at any given location on the landscape might be considered high relative to natural spatial variation. Nonetheless, plot-level estimates of aboveground biomass in tropical forests have reported uncertainties of up to 50% (Keller and others 2001), yet our mapping errors were comparatively low at 20–30% for most closed-canopy forest types. In the less common conditions of very open forest, such as in the poorly drained bog area and the montane, native woodland, our errors did reach 200% of the mean, indicating that a different set of lidar-AGB equations are ultimately needed for these open systems. An explicit accounting of fractional canopy cover changes in the lidar data might be very useful in this context (Lefsky and others 2002a).

Our greatest source of uncertainty was in the field-based allometrics that resulted in relatively large residuals in the lidar-AGB equations shown in Figure 6. The uncertainties in the field measurements appeared primarily related to variation in DBH measurements among field teams (data not shown), but particularly in the field-based estimates of tree height, which are exceedingly difficult to make in tall, closed-canopy forest. In addition, an unknown amount of the error in the lidar-AGB equations is caused by stochastic error in the lidar vertical profiles, in terms of the number and configuration of the vegetative surfaces intercepted by the laser, and the ability of the lidar to penetrate to the ground level. Our lidar was operated at 50 kHz with 1.25 m spot spacing and 35–40% overlap between flightlines. This results in a very high data point density, providing generally reliable canopy penetration (Asner and others 2007; Asner and others 2008). Nonetheless, the ability to validate 3-D profiles and canopy penetration in closed-canopy forest conditions is limited, and likely represents a continuing source of error as reported previously (Drake and others 2003; Popescu and others 2004).

Among the most powerful aspects of using high pulse-rate lidar to map biomass is the ability to cover large forested areas—in this case, more than 5,000 ha in a few hours of flight—to derive a map of relative structural changes in forest canopies across the landscape (Lefsky and others 2002b). Subsequent canopy profile metrics derived from lidar, especially those that weight the lidar returns vertically (Figures 4–5; Table 3) (Lefsky and others 2002a), are easy to apply, and provide reasonable AGB estimates in comparison to plot-level measurements. In Hawaiian forests, the uncertainties in lidar-based mapping can be decreased over time as species-specific allometric equations are developed (for example, Raich and others 1997; Aplet and others 1998). We often lacked species-level allometric data, so we relied on the general ''Wet Forest'' equation of Chave and others (2005), which proved to be very useful. In fact, we used the Chave and others (2005) equation for *F. uhdei*, only to find out that a specific equation had recently been developed for this species by D. Rothstein (*unpub. data*). After applying his equation to the plots containing *F. uhdei*, we found a 99% correlation between the generic and specific allometrics. Still, this may not be the case for other species encountered in Hawaiian forests, and additional field research is needed.

## Conclusions

This study combined field and airborne measurements to map aboveground biomass throughout a rain forest landscape in northeastern Hawaii. Our results show that canopy vertical profiles derived from airborne lidar are well correlated with plot-estimated biomass across a range of elevation (climate), substrate age, and biotic conditions. Our approach provided a unique opportunity to investigate causes of AGB variation across a broad set of conditions, affording a means to assess the relative importance of environmental and biotic factors affecting forest biomass.

We found significant effects of both substrate age and elevation on mean AGB as well as on the spatial variability of biomass within each forest type. Among native *M. polymorpha* stands, a decrease of 1500 mm $y^{-1}$ rainfall and 5°C mean annual temperature was sufficient to cause a 64–84% decrease in AGB levels, depending upon substrate age. Holding climate constant, substrate ages from just 5–65 ky caused a 23–53% decline in biomass, depending upon elevation. Due to interacting effects among these two environmental factors, not to mention local-scale variation in relief, we are unable to quantify the precise relative importance of climate and substrate on biomass across this rain forest reserve. Nonetheless, it appears that climate plays a stronger role than substrate age, at least within this range of environmental conditions.

We found that the proliferation of non-native tree species *P. cattleianum*/*F. rubiginosa* and *F. uhdei* have significant but opposing effects on AGB in Hawaiian rain forests. Our results suggest that the fast-growing invaders decrease average biomass levels and increase the spatial variation in biomass, whereas the slower growing species increase biomass stocks. Moreover, substrate age (soil fertility) and climate mediate the magnitude of biomass change following invasion. Additional studies are needed to quantify the potential carbon gains or losses associated with the rapid transformation of Hawaiian rain forests caused by invasion. New landscape-level studies on the environmental and biotic causes of biomass change will eventually aid in developing strategies for the increased sequestration of carbon for climate change mitigation.

## ACKNOWLEDGMENTS

We thank R. Martin, D. Okita, G. Sanchez, and the HETF field crew for field, laboratory, airborne, and/or logistical support. We thank M. Keller for early advice on the study. The Carnegie Airborne Observatory is funded by the W.M. Keck Foundation and William Hearst III. Application of the Carnegie Airborne Observatory to this study was supported by the Carnegie Institution and the USDA Forest Service. Access to field sites was provided by the State of Hawaii Department of Land and Natural Resources-Division of Forestry and Wildlife.

## REFERENCES

Aplet GH, Vitousek PM. 1994. An age-altitude matrix analysis of Hawaiian rain-forest succession. J Ecol 82:137–47.

Aplet GH, Hughes FR, Vitousek PM. 1998. Ecosystem development on Hawaiian lava flows: biomass and species composition. J Veg Sci 9:17–26.

Armstrong RW, Ed. 1983. Atlas of Hawaii. Honolulu: University of Hawaii Press.

Asner GP, Knapp DE, Kennedy-Bowdoin T, Jones MO, Martin RE, Boardman J, Field CB. 2007. Carnegie Airborne Observatory: in-flight fusion of hyperspectral imaging and waveform light detection and ranging (LiDAR) for three-dimensional studies of ecosystems. J Appl Remote Sens 1:doi:10.1117/1111.2794018.

Asner GP, Hughes RF, Vitousek PM, Knapp DE, Kennedy-Bowdoin T, Boardman J, Martin RE, Eastwood M, Green RO. 2008. Invasive plants transform the 3-D structure of rainforests. Proceedings of the National Academy of Sciences 10.1073/pnas.0710811105.

Bhatt YD, Rawat YS, Singh SP. 1994. Changes in ecosystem functioning after replacement of forest by Lantana shrubland in the Kumaun Himalaya. J Veg Sci 5:67–70.

Brown S, Lugo AE. 1984. Biomass of tropical forests: a new estimate based on forest volumes. Science 223:1290–3.

Brown S, Pearson T, Slaymaker D, Ambagis S, Moore N, Novelo D, Sabido W. 2005. Creating a virtual tropical forest from three-dimensional aerial imagery to estimate carbon stocks. Ecol Appl 15:1083–95.

Carlson NK, Bryan LW. 1963. The Honaunau forest: an appraisal after seven years of planting. J For 61:643–7.

Chadwick OA, Derry LA, Vitousek PM, Huebert BJ, Hedin LO. 1999. Changing sources of nutrients during four million years of ecosystem development. Nature 397:491–7.

Chave J, Chust G, Condit R, Aguilar S, Hernandez A, Lao S, Perez R. 2004. Error propagation and scaling for tropical forest biomass estimates. In: Malhi Y, Phillips O, Eds. Tropical forests and global atmospheric change. London: Oxford University Press. p 155–66.

Chave J, Andalo C, Brown S, Cairns MA, Chambers JQ, Eamus D, Fölster H, Fromard F, Higuchi N, Puig H, Riéra B, Yamakura T. 2005. Tree allometry and improved estimation of carbon stocks and balance in tropical forests. Oecologia. doi: 10.1007/s00442–005-0100-x.

Clark DA. 2002. Are tropical forests an important carbon sink? Reanalysis of the long-term plot data. Ecol Appl 12:3–7.

Cordell S, Goldstein G, Mueller-Dombois D, Webb D, Vitousek PM. 1998. Physiological and morphological variation in Metrosideros polymorpha, a dominant Hawaiian tree species, along an altitudinal gradient: the role of phenotypic plasticity. Oecologia (Berlin) 113:188–96.

Crews TE, Kitayama K, Fownes JH, Riley RH, Herbert DA, Mueller-Dombois D, Vitousek PM. 1995. Changes in soil phosphorus fractions and ecosystem dynamics across a long chronosequence in Hawaii. Ecology 76:1407–24.

DLNR. 1989. Laupahoehoe natural area reserve management plan. Natural area reserve system. Honolulu, Hawaii: Department of Land and Natural Resources.

Drake JB, Dubayah RO, Knox RG, Clark DB, Blair JB. 2002. Sensitivity of large-footprint lidar to canopy structure and biomass in a neotropical rainforest. Remote Sens Environ 81:378–92.

Drake JB, Knox RG, Dubayah RO, Clark DB, Condit R, Blair JB, Hofton M. 2003. Above-ground biomass estimation in closed canopy neotropical forests using lidar remote sensing: factors affecting the generality of relationships. Glob Ecol Biogeogr 12:147–59.

Ehrenfeld JG. 2003. Effects of exotic plant invasions on soil nutrient cycling processes. Ecosystems 6:503–23.

Francis JK. 1990. Fraxinus uhdei (Wenzig) Lingelsh. USDA Forest Service Technical Report SO-ITF-SM–28. USDA Forest Service.

Giambelluca TW, Nullet MA, Schroeder TA. 1986. Rainfall Atlas of Hawaii. Honolulu: Department of Land and Natural Resources, State of Hawaii, p 267.

Houghton RA, Skole DL, Nobre CA, Hackler JL, Lawrence KT, Chomentowski WH. 2000. Annual fluxes of carbon from deforestation and regrowth in the Brazilian Amazon. Science 403:301–4.

Huenneke LF, Vitousek PM. 1990. Seedling and clonal recruitment of the invasive tree Psidium cattleianum: implications for management of native Hawaiian forests. Biol Conserv 53:199–211.

Hughes RF, Kauffman JB, Cummings DL. 2002. Dynamics of aboveground and soil carbon and nitrogen stocks and cycling of available nitrogen along a land-use gradient in Rondonia, Brazil. Ecosystems 5:244–59.

Keller M, Palace M, Hurtt G. 2001. Biomass estimation in the Tapajos National Forest, Brazil: examination of sampling and allometric uncertainties. For Ecol Manag 154:371–82.

Laurance WF, Fearnside PM, Laurance SG, Delamonica P, Lovejoy TE, Rankin-de Merona JM, Chambers JQ, Gascon C. 1999. Relationship between soils and Amazon forest biomass: a landscape-scale study. For Ecol Manag 118:127–38.

Lefsky MA, Cohen WB, Acker SA, Parker GG, Spies TA, Harding D. 1999. Lidar remote sensing of the canopy structure and biophysical properties of Douglas-fir western hemlock forests. Remote Sens Environ 70:339–61.

Lefsky MA, Cohen WB, Harding DJ, Parker GG, Acker SA, Gower ST. 2002a. Lidar remote sensing of above-ground biomass in three biomes. Glob Ecol Biogeogr 11:393–9.

Lefsky MA, Cohen WB, Parker GG, Harding DJ. 2002b. Lidar remote sensing for ecosystem studies. Bioscience 52:19–30.

Lefsky MA, Harding DJ, Keller M, Cohen WB, Carabajal CC, Espirito-Santo FDB, Hunter MO, Oliveira R Jr. 2005. Estimates of forest canopy height and aboveground biomass using ICESat. Geophys Res Lett 32:L22S02. doi:10.1029/2005GL023971.

Morsdorf F, Kotz B, Meier E, Itten KI, Allgower B. 2006. Estimation of LAI and fractional cover from small footprint airborne laser scanning data based on gap fraction. Remote Sens Environ 104:50–61.

Mueller-Dombois D. 1987. Natural dieback in forests. Bioscience 37:575–83.

Palace M, Keller M, Asner GP, Hagen S, Braswell B. 2008. Amazon forest structure from IKONOS satellite data and the automated characterization of forest canopy properties. Biotropica 40:141–50.

Phillips OL, Mahli Y, Higuchi N, Laurance WF, Núñez PV, Vázquez RM, Laurance SG, Fereira LV, Stern M, Brown S, Grace J. 1998. Changes in the carbon balance of tropical forests: evidence from long-term plots. Science 282:439–42.

Phillips OL, Malhi Y, Vinceti B, Baker T, Lewis SL, Higuchi N, Laurance WF, Vargas PN, Martinez RV, Laurance S, Ferreira LV, Stern M, Brown S, Grace J. 2002. Changes in growth of tropical forests: evaluating potential biases. Ecol Appl 12:576–87.

Popescu SC, Wynne RH, Scrivani JA. 2004. Fusion of small-footprint lidar and multispectral data to estimate plot-level volume and biomass in deciduous and pine forests in Virginia, USA. Forest Sci 50:551–65.

Porder S, Paytan A, Vitousek PM. 2005. Erosion and landscape development affect plant nutrient status in the Hawaiian Islands. Oecologia (Berlin) 142:440–9.

Raich JW, Russell AE, Vitousek PM. 1997. Primary productivity and ecosystem development along an elevational gradient on Mauna Loa, Hawaii. Ecology 78:707–22.

Raich JW, Russell AE, Kitayama K, Parton WJ, Vitousek PM. 2006. Temperature influences carbon accumulation in moist tropical forests. Ecology 87:76–7.

Reyes G, Brown S, Chapman J, Lugo AE. 1992. Wood densities of tropical tree species. In: Service USF, Ed. U.S. Department of Agriculture, p 18.

Rothstein DE, Vitousek PM, Simmons BL. 2004. An exotic tree alters decomposition and nutrient cycling in a Hawaiian montane forest. Ecosystems 7:805–14.

Smith CW. 1985. Impact of alien plants on Hawaii's native biota. In: Stone CP, Scott JM, Eds. Hawaii's terrestrial ecosystems: preservation and management. University of Hawaii, Honolulu: Cooperative National Park Resources Study Unit. p 180–250.

Stearns HT. 1985. Geology of the State of Hawaii. Palo Alto: Pacific Books, p 335.

Treuhaft RN, Law BE, Asner GP. 2004. Forest attributes from radar interferometric structure and its fusion with optical remote sensing. Bioscience 54:561–71.

Vitousek PM. 2004. Nutrient cycling and limitation: Hawai'i as a model system. Princeton, NJ: Princeton University Press, p 232.

Vitousek PM, Chadwick OA, Crews TE, Fownes JH, Hendricks DM, Herbert D. 1997. Soil and ecosystem development across the Hawaiian Islands. GSA Today 7:1–8.

Zimmerman N, Hughes RF, Cordell S, Hart P, Chang HK, Perez D, Like RK, Ostertag R. 2007. Patterns of primary succession of native and introduced plants in lowland wet forests in Eastern Hawaii. Biotropica doi:10.1111/j.1744-7429.2007.00371.x.